

Fast Mølmer-Sørensen gates in trapped-ion quantum processors with compensated carrier transition

Evgeny Anikin,¹ Andrey Chuchalin,^{1,2} Nikita Morozov,¹ Olga Lakhmanskaya,¹ and Kirill Lakhmanskij¹

¹*Russian Quantum Center, Skolkovo, Moscow 143025, Russia*

²*Moscow Institute of Physics and Technology, Dolgoprudny, 141700, Russia*

(Dated: April 10, 2025)

Carrier transition is one of the major factors hindering the high-speed implementation of the Mølmer-Sørensen gates in trapped-ion quantum processors. We present an approach to design laser pulse shapes for the Mølmer-Sørensen gate in ion chains which accounts for the effect of carrier transition on qubit-phonon dynamics. We show that the fast-oscillating carrier term effectively modifies the spin-dependent forces acting on ions, and this can be compensated by a simple nonlinear transformation of a laser pulse. Using numerical simulations for short ion chains and perturbation theory for longer chains up to 20 ions, we demonstrate that our approach allows to reach the infidelity below 10^{-4} while keeping the gate duration of the order of tens of microseconds.

I. INTRODUCTION

High-fidelity entangling gates are critical for the practical realization of quantum computers. With cold trapped ions, remarkable progress in such gate implementation has been achieved in recent decades [1]. Since the Cirac-Zoller gate [2], various gate designs have been proposed and implemented, including Mølmer-Sørensen gate [3], light-shift gate [4], ultrafast gates [5], etc. Among them, the Mølmer-Sørensen gate and its variations are the most ubiquitous.

The Mølmer-Sørensen gate MS gate is implemented with the help of a bichromatic external field pulse detuned symmetrically from the qubit transition, typically optical or Raman [3]. In the Lamb-Dicke regime, the field creates a spin-dependent force acting on ions, and the pulse parameters should be chosen to make ion trajectories closed curves in phase space. As a result, qubits acquire a spin-dependent phase and become entangled.

For a two-ion crystal, high-fidelity MS gates can be implemented with constant-amplitude field smoothly turned on and off [6]. For larger ion number, more complicated pulse shapes are required in order to close phase space trajectories for multiple motional modes of an ion crystal [7]. For amplitude-modulated pulses, the pulse shape is determined by a set of linear equations [7] which can be efficiently solved numerically.

In recent literature, a variety of pulse shaping approaches have been proposed for different purposes. Apart from amplitude modulation proposed in [7], phase modulation [8] and multi-tone beams [9] can be used. Also, additional constraints on the pulse shape allow to implement parallel gates [10, 11], to enhance gate robustness against fluctuations of the experimental parameters [12, 13], or to minimize the total external field power [12].

A careful error analysis is necessary to design laser pulses implementing MS gate with highest possible fidelity. The errors originate both from technical noises, such as laser and magnetic field fluctuations, and the intrinsic laser-ion interactions [14]. To account for the

latter, it is necessary to go beyond the usual simplifying assumptions such as Lamb-Dicke and rotating-wave approximations often used to describe laser-ion dynamics. The latter can be achieved by a numerical simulation in the full ion-phonon Hilbert space or by applying a systematical procedure such as Magnus expansion beyond the leading order [15, 16].

One of the unwanted interactions affecting the trapped-ion dynamics during the gate operation is the carrier transition [14]. For MS gate operation, the bichromatic beam components should be tuned closely to qubit motional sidebands. However, due to finite gate duration, the off-resonant direct (carrier) transition between qubit levels is also present. Its influence on the gate dynamics depends significantly on the type of the laser beam configuration. For example, the recent implementation of the MS gate with a phase-stable standing wave [17] allows to eliminate carrier transition almost entirely. Also, for Raman qubits in phase-insensitive geometry [18], carrier transition causes only an additional spin-dependent phase. However, carrier transition significantly contributes into gate dynamics for two widely used beam configurations: for a single bichromatic beam with two co-propagating components and for Raman qubits in phase-sensitive geometry. In these cases carrier transition adds as a non-commuting term to the spin-dependent force Hamiltonian. Although its presence can be utilized to create new types of interactions between ion qubits [19], carrier term becomes one of the dominant factors limiting gate fidelity at short gate durations.

The theoretical analysis of ion dynamics with full account of non-commuting carrier term has been performed for two ions interacting with a single phonon mode [6, 19, 20]. It has been shown that the fast-oscillating carrier term results in a nonlinear renormalization of the driving field amplitude, and (for strictly rectangular pulse) in a basis rotation of the $R_{XX}(\theta)$ gate operator depending on the relative phase between the bichromatic beam components. However, such analysis has not been performed for longer ion chains where the dynamics of multiple phonon modes should be considered.

In this work, we present a theoretical analysis of the influence of carrier transition on MS gate dynamics in an ion chain with account of all phonon modes. Our analysis applies to a bichromatic beam with two co-propagating components, which corresponds to the cases of optical qubits and Raman qubits in phase-sensitive geometry. For amplitude-shaped pulse, we eliminate the carrier term in the system Hamiltonian by transitioning into the interaction picture. The leading part of the resulting Hamiltonian has the form of a spin-dependent force Hamiltonian, where carrier transition modifies the force values obtained from Lamb-Dicke expansion. We propose a family of pulse shapes which take this modification into account. Our pulses can be found by applying a simple nonlinear transformation to a pulse obtained from linear equations. We use numerical simulations for short chains and perturbation theory calculations for longer chains to demonstrate that our pulse shaping scheme shows a considerable fidelity gain in comparison to the pulses obtained from linear equations. In particular, we demonstrate the theoretical infidelity below 10^{-4} for our pulses for 2-20 ions in the chain.

So, our pulse shaping approach provides a considerable speedup while maintaining high gate fidelity, which is an important step towards meeting the challenging requirements for practical quantum computations.

II. DYNAMICS OF TRAPPED IONS QUBITS IN THE PRESENCE OF CARRIER TRANSITION

We consider a trapped-ion quantum processor consisting of a system of ions confined in a radio frequency Paul trap irradiated by laser light. Two electronic levels of each ion constitute the qubit levels. We assume that the ions form a linear crystal, therefore, ions share independent sets of collective phonon modes for each trap axis direction [21]. We consider the implementation of an entangling gate between two ion qubits, namely Mølmer-Sørensen gate (MS gate) [3]. For that, bichromatic laser field symmetrically detuned from qubit transition is required, and we focus on the case of amplitude-modulated field. The interaction-picture Hamiltonian for the considered pair of ions reads [22]

$$\begin{aligned} \hat{H} &= -i \sum_{i=1,2} \Omega(t) \cos(\mu t + \psi) (e^{ik_a \hat{r}_{ia}} \sigma_+^i - \text{h.c.}), \\ k_a \hat{r}_{ia} &= \sum_{m=1}^{n_{\text{ions}}} \eta_{im} (\hat{a}_m e^{-i\omega_m t} + \hat{a}_m^\dagger e^{i\omega_m t}), \end{aligned} \quad (1)$$

where k_a are the components of the laser field wavevector, \hat{r}_{ia} are the components of ions displacements from their equilibrium positions, \hat{a}_m^\dagger and \hat{a}_m are the creation and annihilation operators $\hat{a}_m, \hat{a}_m^\dagger$ of the phonon modes, ω_m are the phonon mode frequencies, η_{im} are the Lamb-Dicke parameters, $\Omega(t)$ is the bichromatic beam amplitude envelope, and μ is the detuning between the bichromatic beam components. The action of our target MS

gate operator on ion qubits is represented by an operator $R_{XX}(\phi) = \exp\{-i\phi\sigma_x \otimes \sigma_x\}$. For gate implementation, one should find a pulse shape $\Omega(t)$ so that the system evolution operator reduces to the target gate operator.

Typically, the approximate evolution operator is found from the expansion of the system Hamiltonian in the Lamb-Dicke parameters [22]. Up to the first order in the expansion, the Hamiltonian reads

$$\hat{H} \approx \hat{H}_{\text{LD}} = \hat{H}_0 + \hat{H}_1, \quad (2)$$

where

$$\hat{H}_0 = \sum_{i=1,2} \Omega(t) \cos(\mu t + \psi) \sigma_y^i. \quad (3)$$

$$\begin{aligned} \hat{H}_1 &= \sum_{i=1,2} \sum_{m=1}^{n_{\text{ions}}} \eta_{im} \Omega(t) \cos(\mu t + \psi) \times \\ &\quad \times (\hat{a}_m e^{-i\omega_m t} + \hat{a}_m^\dagger e^{i\omega_m t}) \sigma_x^i \end{aligned} \quad (4)$$

The Hamiltonian (2) in the Lamb-Dicke approximation (LD Hamiltonian) contains two terms. The term \hat{H}_1 is a spin-dependent force Hamiltonian [23, 24]. The term \hat{H}_0 (carrier term) corresponds to direct carrier transitions. The contribution of the carrier term is often neglected. This approximation is valid when μ is close to one or several phonon mode frequencies, so \hat{H}_1 contains slowly-oscillating terms which contribute the dynamics significantly, whereas \hat{H}_0 is fastly oscillating. Further, we keep both terms and analyze the contribution of \hat{H}_0 to gate dynamics.

The evolution operator for the spin-dependent force Hamiltonian \hat{H}_1 reads [24]

$$\begin{aligned} \hat{U}_{\text{MS}}(t_1, t_2) &= \exp \left(-\frac{i}{2} \sum_{i,j} \chi_{i,j}^0(t_2, t_1) \sigma_x^i \sigma_x^j \right) \\ &\quad \prod_m D_m \left(\sum_i \sigma_x^i \alpha_{i,m}^0(t_2, t_1) \right), \end{aligned} \quad (5)$$

where

$$\alpha_{im}^0(t_2, t_1) = -i \int_{t_1}^{t_2} f_{im}^0(t') dt' \quad (6)$$

$$\chi_{ij}^0(t_2, t_1) = 2 \text{Re} \int_{t_1}^{t_2} \alpha_{im}^0(t', t_1) (f_{jm}^0)^*(t') dt', \quad (7)$$

$$f_{im}^0(t) = \eta_{im} e^{i\omega_m t} \Omega(t) \cos(\mu t + \psi). \quad (8)$$

An appropriate pulse shape $\Omega(t)$ should be found for the implementation of an $R_{XX}(\theta)$ gate. Let $\Omega(t)$ be applied in the time interval (t_0, t_f) . The evolution operator (5) reduces to the target $R_{XX}(\phi)$ operator provided that

the following conditions for the displacement amplitudes α_{im}^0 and the spin coupling phases χ_{ij}^0 are satisfied [7, 24]:

$$\alpha_{im}^0(t_f, t_0) = 0, \quad (9)$$

$$\chi_{12}^0(t_f, t_0) = \phi. \quad (10)$$

The equations (9) comprise a homogeneous system of $2n_{\text{ions}}$ linear equations for $\Omega(t)$. They can be solved numerically by standard linear algebra routines and define $\Omega(t)$ up to a normalization constant. The latter can be found from the quadratic equation (10). With approximations made, the resulting $\Omega(t)$ implements the MS gate with 100% fidelity.

However, the contribution of the carrier term \hat{H}_0 into infidelity grows with increasing gate speed even in the absence of technical noises. To account for the carrier term systematically, let us switch into the interaction picture with respect to H_0 :

$$|\psi\rangle = e^{-i\int_{t_0}^t \hat{H}_0(t')dt'} |\psi_{Ic}\rangle = e^{-i\Phi(t) \sum_i \sigma_y^i} |\psi_{Ic}\rangle, \quad (11)$$

where

$$\Phi(t) = \int_{t_0}^t dt' \Omega(t') \cos(\mu t' + \psi). \quad (12)$$

After this transformation the Hamiltonian takes the form

$$\begin{aligned} \hat{H}_{Ic} &= \hat{H}_{Ic}^{(0)} + \hat{V} = \\ &= \sum_{i,m} \eta_{im} \Omega(t) \cos(\mu t + \psi) (\hat{a}_m e^{-i\omega_m t} + \hat{a}_m^\dagger e^{i\omega_m t}) \times \\ &\quad \times \underbrace{(\cos 2\Phi(t) \sigma_x^i)}_{\text{leading-order}} + \underbrace{\sin 2\Phi(t) \sigma_z^i}_{\text{perturbation}}. \end{aligned} \quad (13)$$

The transformation (11) is equivalent to the single-qubit rotations applied after the gate operation. These rotations could be compensated by applying additional resonant pulses after the gate operation. However, this is not necessary because the rotation angle $\Phi(t_f)$ can be greatly reduced by choosing such pulse $\Omega(t)$ that satisfies the following smoothness conditions:

1. $\Omega(t)$ varies slowly in comparison to μ^{-1} ,
2. $\Omega(t)$ and its first derivatives vanish at the beginning and at the end of the pulse.

Under these conditions and with our proposed pulse design (described in more detail in subsequent sections), we get typical values of $\Phi(t_f)$ of the order of 10^{-5} - 10^{-4} . Therefore, we can assume that the final state of the qubit-phonon system is determined only by evolution with the Hamiltonian (13).

For further analysis of the Hamiltonian (13), it is convenient to split it into two parts, the leading order part $\hat{H}_{Ic}^{(0)}$ and the perturbation part \hat{V} , as shown by underbraces in Eq. (13). Such a decomposition is justified under two assumptions on $\Phi(t)$:

1. $\Phi(t)$ oscillates near zero;
2. its magnitude remains $\lesssim 1$.

These assumptions hold for all the pulses that will be considered below. With them, the $\cos 2\Phi(t)$ term oscillates near ~ 1 and gives a contribution important on the large timescales. In contrast, $\sin 2\Phi(t)$ oscillates near zero, so its contribution cancels on the large timescales. Because of that, it is reasonable to take the sine term as a perturbation, where $\Phi(t)$ is considered as a small parameter.

The leading-order term $\hat{H}_{Ic}^{(0)}$ has the form of the spin-dependent forces Hamiltonian, so its evolution operator has the same form as (5):

$$\begin{aligned} \hat{U}_0(t_1, t_2) &= \exp \left(-\frac{i}{2} \sum_{i,j} \chi_{i,j}(t_2, t_1) \sigma_x^i \sigma_x^j \right) \\ &\quad \prod_m D_m \left(\sum_i \sigma_x^i \alpha_{i,m}(t_2, t_1) \right), \end{aligned} \quad (14)$$

where

$$\alpha_{im}(t_2, t_1) = -i \int_{t_1}^{t_2} f_{im}(t') dt', \quad (15)$$

$$\chi_{ij}(t_2, t_1) = 2 \operatorname{Re} \int_{t_1}^{t_2} \alpha_{im} f_{jm}^* dt', \quad (16)$$

$$f_{im}(t) = f_{im}^0(t) \underbrace{\cos 2\Phi(t)}_{\text{carrier effect}}. \quad (17)$$

Additional $\cos 2\Phi(t)$ term in $f_{im}(t)$ arises because of the transformation into the interaction picture generated by the carrier term.

The perturbation term \hat{V} generates corrections to the evolution operator. Within the first-order perturbation theory, the evolution operator of the Hamiltonian (13) can be expressed as

$$\hat{U} = \hat{U}_0 \left(\mathbb{1} - i \hat{T}_1 \right), \quad (18)$$

where

$$\hat{T}_1 = \int_{t_0}^{t_f} \hat{U}_0^\dagger(t', t_0) \hat{V} \hat{U}_0(t', t_0) dt'. \quad (19)$$

As the perturbation \hat{V} contains the sigma matrices σ_z^i , the operator \hat{T}_1 causes the spin flip processes in x -basis: for the initial qubit state $|s_1 s_2\rangle_x$ (Pauli string in x -basis), it causes transitions to another Pauli string $|s'_1 s'_2\rangle_x$ which differs from the initial state by a single spin flip. In the next sections, we show that the contribution of \hat{T}_1 into gate dynamics is quite small. Therefore, in the next sections, we use Eq. (14) for pulse shape design, and

Eqs. (18), (19) are used only to calculate contributions to gate infidelity.

With modified expressions for spin-dependent forces, we get new conditions for the implementation of $R_{XX}(\phi)$:

$$\begin{aligned}\alpha_{im}(t_f, t_0) &= 0, \\ \chi_{12}(t_f, t_0) &= \phi.\end{aligned}\quad (20)$$

The definitions of α_{im} and χ_{ij} differ from α_{im}^0 and χ_{ij}^0 by the $\cos 2\Phi(t)$ term, where $\Phi(t)$ is expressed as an integral (12) containing $\Omega(t)$. Because of that, the Eqs. (20) are nonlinear integral equations in contrast to the linear equations (9). In Section (IV), we present a scheme for approximate solution of these equations.

III. CONTRIBUTIONS OF CARRIER TERM TO GATE INFIDELITY

The expressions (14) and (18) for the propagator can be used for analytical calculation of the gate fidelity of an ion chain of arbitrary length. In this section, we present the expressions for the gate fidelity defined in the full ion-phonon Hilbert space. We assume that the ion chain is cooled to the ground state at the beginning of the gate operation, so the initial state of the qubit-phonon system is $|\psi_0\rangle \equiv |\psi_{0q}\rangle \otimes |0_{ph}\rangle$, where $|\psi_{0q}\rangle$ is the initial qubit state. The action of the ideal $R_{XX}(\phi)$ gate turns qubits into the state $R_{XX}(\phi)|\psi_{0q}\rangle$ but leaves all phonon modes in the ground state. Therefore, we can characterize the gate realization by fidelity between the target state $|\psi_t\rangle \equiv R_{XX}(\phi)|\psi_0\rangle$ (the outcome of the ideal $R_{XX}(\phi)$ gate) and the state $|\psi(t_f)\rangle = \hat{U}|\psi_0\rangle$ obtained after the evolution with the Hamiltonian (1):

$$F_{\text{tot}} = |\langle\psi_t|\psi(t_f)\rangle|^2 = |\langle\psi_0|R_{XX}(\phi)^\dagger\hat{U}|\psi_0\rangle|^2. \quad (21)$$

This fidelity definition differs from that of [14], [24] as we do not trace out phonon degrees of freedom. Further, we will analyze different contributions into the total infidelity arising from the presence of the carrier term.

First, we define the fidelity measure F_0 (zero-order fidelity) which quantifies the difference of the leading-order propagator \hat{U}_0 from the target gate:

$$F_0 \equiv |\langle\psi_0|R_{XX}(\phi)\hat{U}_0|\psi_0\rangle|^2 \quad (22)$$

In Appendix A, we find F_0 for various initial states $|\psi_{0q}\rangle$. In particular, for $|\psi_{0q}\rangle = |s_1s_2\rangle_z$ (Pauli strings in the z -basis, $s_i = \pm 1$), the infidelity reads

$$1 - F_0 \approx \sum_{im} |\alpha_{im}(t_f)|^2 + \Delta\chi_{12}(t_f)^2, \quad (23)$$

where $\Delta\chi_{12}(t_f) = \phi - \chi_{12}(t_f)$ is the error in the spin coupling phase. We see that incomplete closure of the phase trajectories and the error in the spin coupling phase give two additive contributions into the average gate infidelity.

For $|\psi_{0q}\rangle = |s_1s_2\rangle_x$ (Pauli strings in x -basis), zero-order gate infidelity is given by expression

$$1 - F_0 = P_{\text{ph}}^s = \sum_m \left| \sum_i \alpha_{im} s_i \right|^2. \quad (24)$$

In this case, the error in ϕ does not contribute to gate fidelity. At small α_{im} , the infidelity can be interpreted as the probability of phonon excitation after the gate operation.

Second, we determine the contribution to infidelity P_{flip}^s caused by the spin-flip perturbation accounted by the \hat{T}_1 term in the evolution operator (18). For simplicity, we consider only the initial states $|\psi_0\rangle = |s_1s_2\rangle_x$. The spin flip probability for such initial states is

$$P_{\text{flip}}^s = \langle s, 0_{\text{ph}} | \hat{T}_1^\dagger \hat{T}_1 | s, 0_{\text{ph}} \rangle. \quad (25)$$

In Appendices A and B, we derive the explicit expression (B8) for P_{flip}^s as a two-dimensional integral over time. (The Eq. (B8) is too long to present it in the main text.) The integral (B8) is suitable for the calculation of the spin flip probability for long ion chains where the full numerical solution is not feasible. Also, we show that the gate infidelity for the initial states $|s_1s_2\rangle_x$ with account of the carrier transition reads

$$1 - F_{\text{tot}} = P_{\text{ph}}^s + P_{\text{flip}}^s, \quad (26)$$

so the contributions of imperfectly closed phase trajectories and spin flip error are additive. For other qubit states, there are interference terms between the two considered contributions.

Finally, we derive an upper bound for the infidelity averaged over all initial qubit states over the Fubini-Study measure [25]:

$$1 - \langle F_{\text{tot}} \rangle < 1 - \langle F_0 \rangle + \frac{1}{4} \sum_s P_{\text{flip}}^s, \quad (27)$$

where F_0 given by Eq. (22) accounts only for the leading-order term of \hat{U} . Therefore, it is sufficient to calculate the contribution of \hat{T}_1 only for the initial states $|s_1s_2\rangle_x$ to find an upper bound for the average gate infidelity.

Thus, carrier term contributes into two types of gate error. First, it modifies the values of the spin-dependent forces, so it causes incomplete closing of the phase trajectories unless the pulse shape is chosen appropriately. Second, it causes the spin-flip error arising from \hat{T}_1 . In the following, we present a method to find pulse shapes which minimize the error of the first kind.

IV. COMPENSATION OF CARRIER ERROR BY A TRANSFORMATION OF AN AMPLITUDE-SHAPED PULSE

In this section, we present a method to find pulse shapes as approximate solutions of the Eqs. (20). This

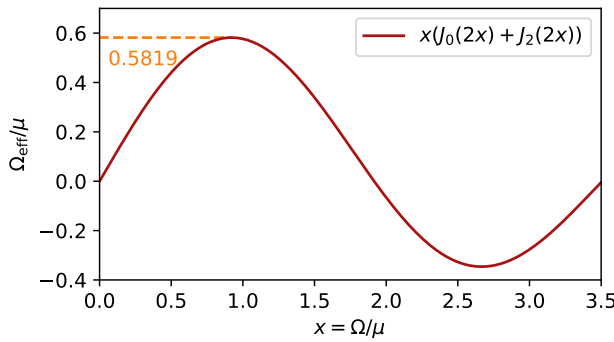


Figure 1. (a) The dependence of the effective Rabi frequency $\Omega_{\text{eff}}(t)$ on Ω given by Eq. (29).

compensates the modification of the spin-dependent forces by the carrier term and increases the gate fidelity. First, we describe the method itself in the subsection (IV A). Then, we demonstrate its performance on a particular example of a 5-ion chain in (IV B). We show that our method offers a significant fidelity gain in comparison with the pulse obtained from the linear Eqs. (9), (10), which are used in the most of the pulse shaping approaches. After that, in the subsection IV C, we study the applicability of our method for other gate durations, chain lengths, and values of bichromatic detuning.

A. Pulse shaping scheme

Assuming that $\Omega(t)$ satisfies the smoothness conditions from Section II, the $\cos 2\Phi(t)$ term in Eq. (17) can be averaged over fast oscillations on the timescale μ^{-1} , as shown in Appendix C. As a result, we get an approximate expression for f_{im} in Eq. (17):

$$f_{im} \approx \eta_{im} e^{i\omega_m t} \Omega_{\text{eff}}(t) \cos(\mu t + \psi), \quad (28)$$

where

$$\Omega_{\text{eff}}(t) = \mathcal{S}(\Omega(t)) = \Omega(t) \left(J_0 \left(\frac{2\Omega(t)}{\mu} \right) + J_2 \left(\frac{2\Omega(t)}{\mu} \right) \right), \quad (29)$$

and J_k are Bessel functions. So, the $\cos 2\Phi(t)$ term in Eqs.(15), (16) causing the nonlinearity of Eqs. (20) disappears. Thus, α_{im} and χ_{ij} can be calculated with Eqs. (6), (7) as there were no carrier term, but with $\Omega(t)$ replaced by $\Omega_{\text{eff}}(t)$.

The transformation $\mathcal{S}(\Omega)$ given by Eq. (29) can be thought as a nonlinear squeezing transformation of $\Omega(t)$. In Fig. 1, we depict the functional dependence of $\mathcal{S}(\Omega)$ on Ω . When $\Omega \ll \mu$, $\mathcal{S}(\Omega) \approx \Omega$. At larger $\Omega \sim \mu$, $\mathcal{S}(\Omega)$ grows slower than Ω until it reaches its absolute maximum $\max(\mathcal{S}) = C\mu$, where $C \approx 0.581865$. Thus, the presence of the carrier term effectively reduces the field amplitude acting on an ion qubit.

	$\Omega_{\text{tr}}(t)$	$\Omega_{\text{lin}}(t)$
$1 - F_0$	1.4×10^{-6}	1.2×10^{-2}
Num. (LD)	1.7×10^{-6}	1.2×10^{-2}
Num. (full)	5.7×10^{-5}	1.4×10^{-2}

Table I. $R_{\text{XX}}(\pi/4)$ gate fidelity for the pulses Ω_{lin} and Ω_{tr} with the initial state $|11\rangle_z$. The values in the first row are obtained from the analytical expression (23). The values in the second and the third row are obtained from TDSE solution with the Hamiltonians (2) and (1).

Using the transformation (29), we can find approximate solutions $\Omega_{\text{tr}}(t)$ of the nonlinear equations (20) in two simple steps:

1. Find $\Omega_{\text{lin}}(t)$ satisfying Eqs. (9), (10) and smoothness conditions, where α_{im}^0 and χ_{ij}^0 are defined by Eqs. (6), (7), (8). This pulse would implement the $R_{\text{XX}}(\phi)$ gate if the carrier term was not present.
2. Find the solution by applying the inverse transformation \mathcal{S}^{-1} : $\Omega_{\text{tr}}(t) = \mathcal{S}^{-1}(\Omega_{\text{lin}}(t))$. This accounts for the modified expressions for the spin-dependent forces.

B. 5-ion chain example

Let us illustrate the presented pulse shaping scheme on a particular example. We consider a chain of $n_{\text{ions}} = 5$ $^{40}\text{Ca}^+$ ions in a harmonic pseudopotential with the radial frequency of 1 MHz and the axial frequency of 264.8 kHz. The frequency of the lowest radial mode at these parameters is 0.75 MHz. We calculate the ion equilibrium positions, phonon normal modes and frequencies and the Lamb-Dicke parameters of the chain using standard methods (see Fig. 2a-c and Appendix D) [21]. Then, we find the pulses implementing the $R_{\text{XX}}(\phi = \pi/4)$ gate between the second and the third ions of the chain for the gate duration $41.74 \mu\text{s}$, the detuning $\mu = 2\pi \times 1.034 \text{ MHz}$, and the motional phase $\psi = 0$.

We search for $\Omega_{\text{lin}}(t)$ as a smooth piecewise-cubic polynomial (cubic spline) with $2n_{\text{ions}} + 2 = 12$ segments equally spaced in the interval time (t_0, t_f) with $t_0 = 0$ and $t_f = 41.74 \mu\text{s}$. Additionally, we require that the values and the derivatives vanish at the beginning and at the end of the gate. Under these requirements, Eqs. (9), (10) have a unique solution (see Appendix E). To find $\Omega_{\text{tr}}(t)$, we apply the inverse transformation (29). For the considered 5-ion chain, $\Omega_{\text{lin}}(t)$ and $\Omega_{\text{tr}}(t)$ are shown in Fig. 2d.

Then, we compare the system dynamics for $\Omega_{\text{lin}}(t)$ and $\Omega_{\text{tr}}(t)$. Using Eqs. (15), (16), we find $\alpha_{im}(t, t_i)$ and $\chi_{ij}(t, t_i)$ entering the propagator (14) for both pulses. For the center-of-mass (COM) and stretch modes of an ion crystal which are excited the most during the gate operation, the phase trajectories are shown in Fig. 2e, and $\chi_{12}(t)$ is shown in Fig. 2f. From the inset in Fig. 2e, it is

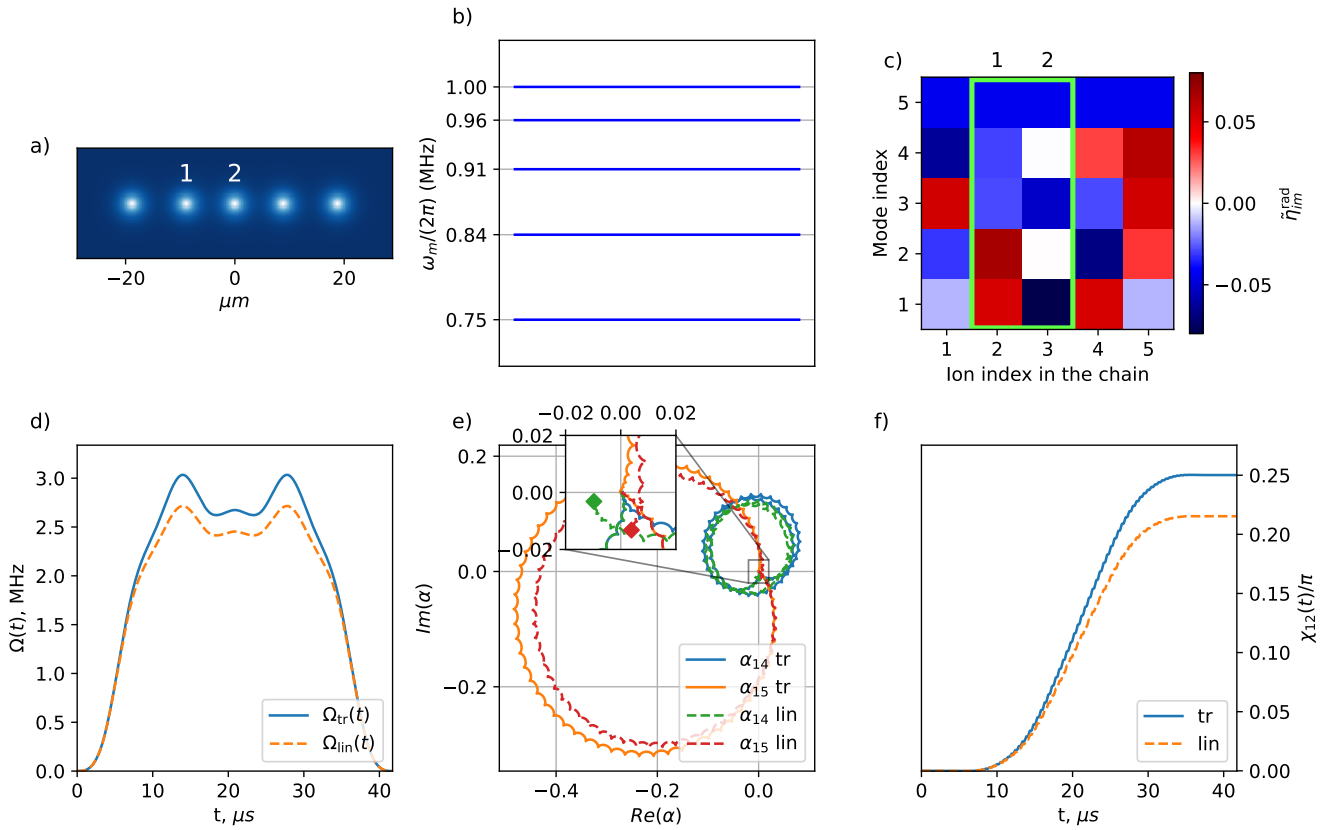


Figure 2. (a) Calculated ion equilibrium positions, (b) radial normal mode frequencies of the chain, and (c) radial Lamb-Dicke parameter matrix for a chain of $^{40}\text{Ca}^+$ ions. The indices 1, 2 in (a) and (c) indicate the ions illuminated by laser field. The green rectangle in (c) indicates two rows of the Lamb-Dicke parameter matrix which correspond to the illuminated ions. (d) Non-optimized and optimized laser pulses applied to ions 1 and 2 indicated in (a). (e) Phase trajectories of the ion 1 for modes 4 (stretch) and 5 (COM) for both pulse shapes. (f) Spin-spin entanglement phase $\chi_{12}(t)$ between the illuminated ions for both pulse shapes.

	Ω_{tr}			Ω_{lin}				
	Eq. (26)		Num. (LD)	Num. (full)	Eq. (26)		Num. (LD)	Num. (full)
	P_{ph}^s	P_{flip}^s	$1 - F_{\text{tot}}$	P_{ph}^s	P_{flip}^s	$1 - F_{\text{tot}}$		
$ 1, 1\rangle_x$	1.9×10^{-6}	8.5×10^{-7}	3.4×10^{-6}	8.8×10^{-4}	9.0×10^{-4}	9.7×10^{-4}		
	9.3×10^{-7}	8.7×10^{-7}	6.6×10^{-6}	3.6×10^{-7}	3.3×10^{-7}	3.6×10^{-6}		
	2.8×10^{-6}	1.8×10^{-6}	1.0×10^{-5}	8.8×10^{-4}	9.0×10^{-4}	9.7×10^{-4}		
$ 1, -1\rangle_x$	6.3×10^{-7}	4.6×10^{-7}	1.1×10^{-6}	1.1×10^{-4}	1.1×10^{-4}	1.0×10^{-4}		
	5.7×10^{-7}	5.3×10^{-7}	3.5×10^{-6}	2.5×10^{-7}	2.2×10^{-7}	2.2×10^{-6}		
	1.2×10^{-6}	1.2×10^{-6}	4.7×10^{-6}	1.1×10^{-4}	1.1×10^{-4}	1.1×10^{-4}		

Table II. Contributions into $R_{XX}(\pi/4)$ gate fidelity for the pulses Ω_{lin} and Ω_{tr} with the initial states $|1, \pm 1\rangle_x$. Each data row of the table corresponds to a contribution to the infidelity with the initial state given in the leftmost column. Each data column of the table corresponds to a calculation method (analytical or numerical with one of the considered Hamiltonians) for the pulse shape given in the top row.

clear that the phonon mode trajectories are not perfectly closed for the pulse $\Omega_{\text{lin}}(t)$ (the phonon mode amplitudes are of the order of $\sim 10^{-2}$ in the end of the gate). In contrast, for $\Omega_{\text{tr}}(t)$ they are almost perfectly closed, and the deviation of the amplitudes from zero is invisible on the plot. Also, the deviation of χ_{12} at the end of the gate is significant for $\Omega_{\text{lin}}(t)$, as opposed to $\Omega_{\text{tr}}(t)$ (invisible

on the plot). Then, we use the abovementioned results to calculate the zero-order infidelity F_0 (Eq. (23)) for the initial states $|11\rangle_z$. The results are presented in Table I. One can see that the theoretical infidelity for the pulse Ω_{tr} is $\sim 10^{-6}$, whereas the infidelity for the pulse Ω_{lin} is of the order of 10^{-2} .

We verify our analytical predictions by solving nu-

merically the time-dependent Schrödinger equation (TDSE) for the full Hamiltonian (1) using QuTiP [26]. The calculated infidelities for both pulses are also in Table I. Qualitatively, the numerical results confirm our analytical prediction that the transformed pulse greatly reduces the gate error. Quantitatively, we obtain good agreement for Ω_{lin} and slightly larger discrepancies for Ω_{tr} . We attribute the difference for Ω_{tr} to the influence of the higher-order terms in the Lamb-Dicke expansion, which are not accounted in our calculations but are present in the full Hamiltonian. To confirm this, we solve TDSE for the LD Hamiltonian (2) where the higher-order terms of the expansion are neglected. The resulting infidelities, also presented in Table I, show much better agreement with the analytical predictions.

Similarly, we analyze the gate fidelity for the initial states $|1, \pm 1\rangle_x$. For these states, Eq. (26) allows to separate the contributions of imperfectly closed phase trajectories and spin flips. These contributions can be identified from the numerical solution of TDSE: the probability of phonon mode excitation corresponds to the first term in Eq. (26), and the probability of the spin flip corresponds to the second term in Eq. (26). In Table II, we present the results of analytical calculations and the TDSE solution both with Hamiltonians (1) and (2).

The results confirm that the first-order perturbation theory in \hat{V} gives an accurate description of the dynamics of the LD Hamiltonian. We obtain good agreement between the analytical and numerical predictions for all cases except for the P_{ph}^s for the transformed pulse. Even in this case, the analytical formula correctly predicts the very small magnitude of phonon excitation probability $\sim 10^{-6}$.

In the simulation of the full Hamiltonian (1) with pulses Ω_{lin} , the considered contributions into error also agree with the analytical predictions. However, for Ω_{tr} , both of the contributions are by order of magnitude larger than the corresponding analytical predictions. Still, the total error for Ω_{tr} is more than by order of magnitude lower than for Ω_{lin} .

From these results, we conclude that the dominant contributions into gate error for Ω_{lin} are the error $\Delta\chi_{12}$ in the spin coupling phase and the imperfect closing of the phase trajectories as in Eq. (23). Both of these contributions can be almost canceled by transforming Ω_{lin} into Ω_{tr} . The spin-flip contribution into error is negligible for both pulses. Thus, the pulse Ω_{tr} allows the implementation of a fast high-fidelity $R_{XX}(\pi/4)$ gate in a 5-ion chain.

C. Gate time, detuning, and chain length dependencies

Here we examine the applicability of the method for other gate durations, detunings, and chain lengths. Below, we find the parameter domains for which the method of Section IV is applicable. For the 5-ion chain considered

previously, we perform analytical and numerical calculations for different parameter values and study the fidelity dependence on these parameters. For longer ion chains, we perform only analytical calculations because they require an exponentially growing amount of computational resources for numerical modelling.

A key point for the implementation of our scheme is the existence of the inverse transformation \mathcal{S}^{-1} . As shown in the subsection IV A (see Eq. (29) and Fig. 1), the effective field amplitude Ω_{eff} has an absolute maximum of $C\mu$: therefore, \mathcal{S}^{-1} is defined only in the range $(-C\mu, C\mu)$. So, for the step 2 of the pulse shaping procedure in the subsection IV A, it is necessary that the absolute value of Ω_{lin} obtained from linear equations does not exceed $C\mu$. This requirement poses a restriction on the possible values of the system and the gate parameters.

The pulse shapes Ω_{lin} obtained from linear equations Eq. (9), (10) depend on the number of ions, the values of normal mode frequencies, the Lamb-Dicke parameters, the detuning of the bichromatic beam, and the gate duration. The normal mode frequencies and the Lamb-Dicke parameters depend on the trap frequencies, ion masses and the wavevectors. However, these dependencies are rather simple and do not contain fast oscillating contributions. The dependence on the motional phase ψ is weak provided that the field amplitude is smoothly turned on and off. In contrast, the dependence on the gate time t_{gate} and μ is highly non-trivial because they enter the pulse shaping equations inside the oscillatory integrals (E2).

Therefore, we mostly focus on the dependence on t_{gate} and μ . We find the sets in the plane (t_{gate}, μ) where \mathcal{S}^{-1} exists (Ω_{lin} does not exceed $C\mu$), which we call the allowed areas (see Fig. 3). Due to complicated dependence of Ω_{lin} on t_{gate} and μ , the allowed areas have complicated shape in the $t_{\text{gate}}-\mu$ plane.

First, we find the allowed area (see Fig. 3a) for the 5-ion chain considered in the previous section. We calculate $\Omega_{\text{lin}}(t)$ for a (1450×800) grid in $t_{\text{gate}}-\mu$ plane for gate durations from 5 to 150 μs and detunings from 0.6 to 1.2MHz. Along the vertical axis, the area occupies the values of μ lying closely to the band of radial phonon frequencies. Along the horizontal axis, it spans the whole range of t_{gate} except the values below $\sim 30\mu\text{s}$. For each grid point inside the allowed area, we calculate the transformed pulse $\Omega_{\text{tr}}(t)$. Using Eq. (23), we calculate the leading-order contribution $1 - F_0$ to gate infidelity for the initial state $|11\rangle_z$ for each pair t_{gate}, μ . The result is shown by color inside the allowed area in Fig. 3a. We find that infidelity is of the order of 10^{-5} nearly for all the grid points inside the area except the vicinity of the boundaries.

For comparison, we calculate $1 - F_0$ for pulses Ω_{lin} for the initial state $|11\rangle_z$ for the entire grid. The result is shown in Fig 3(c). We find that the infidelity for Ω_{lin} is of the order of $10^{-3}\text{-}10^{-2}$ inside the allowed area, which is considerably larger than the infidelity for Ω_{tr} . Outside the allowed area, the error reaches $\sim 10^{-1}$ and even more

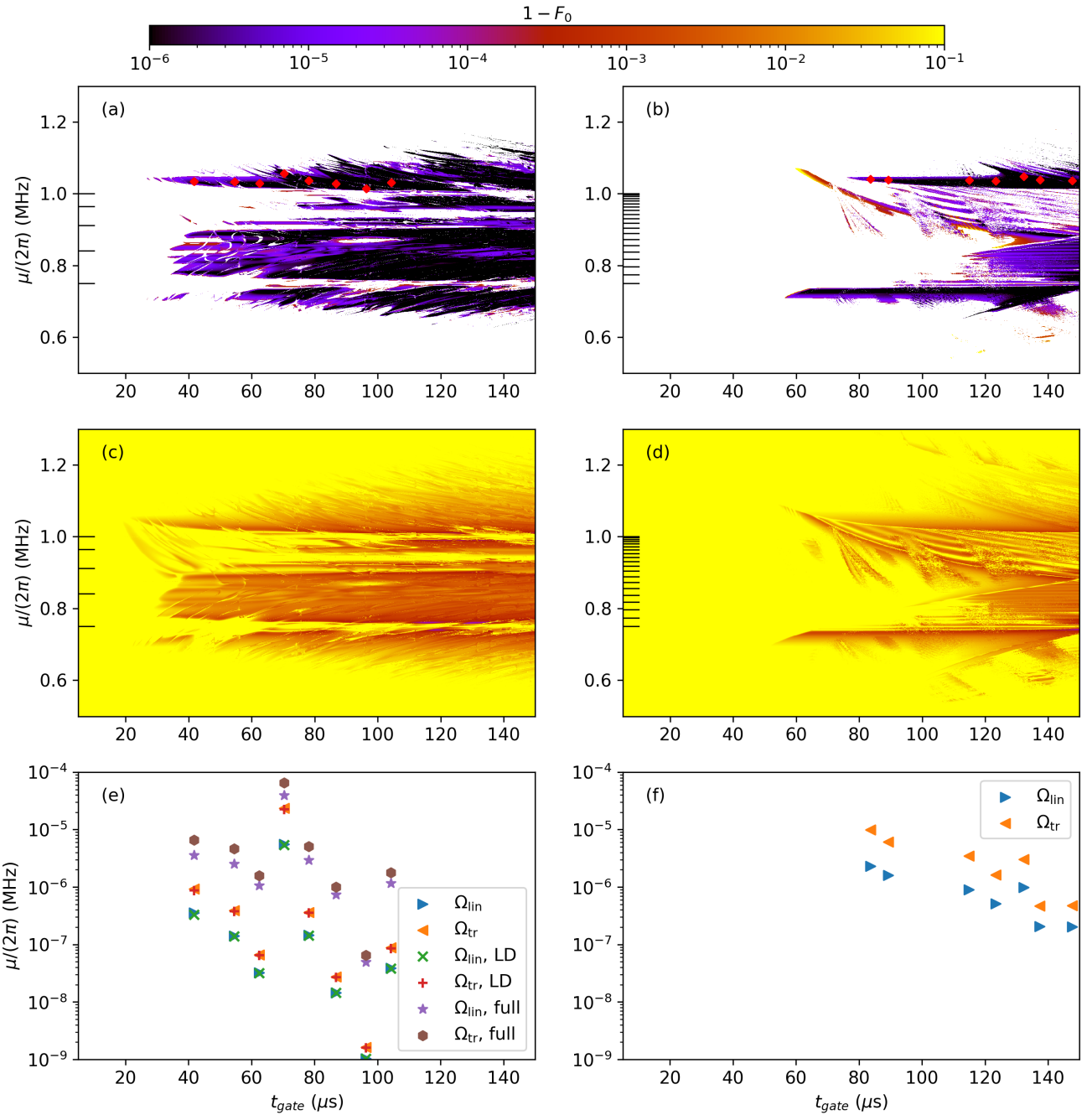


Figure 3. (a,b) Leading-order infidelity $1 - F_0$ (indicated by color) for transformed pulses Ω_{tr} inside the area where the inverse transformation \mathcal{S}^{-1} exists for 5-ion (a) and 20-ion (b) chains. White color outside the allowed area indicates that \mathcal{S}^{-1} is not defined. The red dots specify the values of (t_{gate}, μ) for which the simulations are performed. (c, d) Leading-order infidelity $1 - F_0$ for non-transformed pulses Ω_{lin} for 5-ion (a) and 20-ion (b) chains. The black horizontal lines in (a-d) indicate the positions of normal mode frequencies. (e) Spin flip error for the initial state $|11\rangle_x$ of a 5-ion chain with (t_{gate}, μ) labeled by dots in (a). It is calculated analytically and numerically with the LD and full Hamiltonians for transformed and non-transformed pulses. (f) Analytical spin flip error for the initial state $|11\rangle_x$ of a 5-ion chain with (t_{gate}, μ) specified by dots in (b).

due to larger values of Ω_{lin} .

We repeat these calculations for a 20-ion chain (see the results in Fig. 3(b,d)). All laser and trap parameters are taken the same as for the 5-ion case except

the axial frequency and the number of segments in the pulse. The number of segments in the pulse is enlarged to $2n_{\text{ions}} + 1 = 41$. The axial frequency is set to 78.7 kHz, which results in radial phonon modes lying in

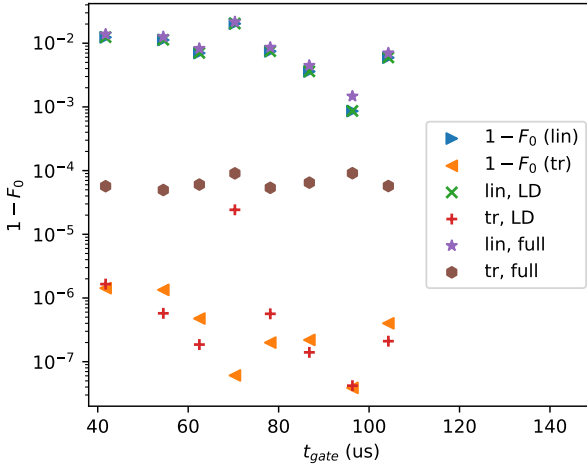


Figure 4. Leading-order infidelity $1 - F_0$ compared with the infidelity calculated from numerical simulation for the initial state $|11\rangle_z$ in 5-ion chain with t_{gate}, μ specified in Fig. 3(a). The values of $1 - F_0$ are compared with the simulation results for the LD Hamiltonian and full Hamiltonian both for transformed and non-transformed pulses.

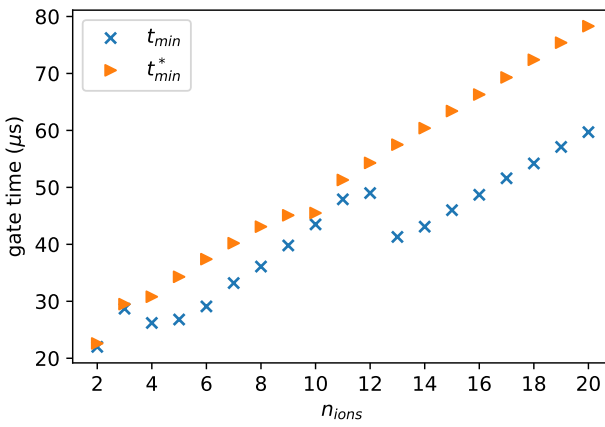


Figure 5. Minimal gate duration t_{min} for which Ω_{eff} does not exceed $C\mu$ and minimal gate duration t_{min}^* ensuring the zero-order error equal to 10^{-5} for optimized pulses and $|\psi_0\rangle = |11\rangle_z$ as functions of n_{ions} .

the range (0.75MHz, 1MHz) similarly to the 5-ion case. In Fig. 3(b,d), we show the results for a 20-ion chain. Analogously to the 5-ion case, we find the allowed area and calculate $1 - F_0$ for Ω_{lin} and Ω_{tr} in the t_{gate}, μ plane. The 20-ion allowed area (see Fig. 3(b)) has a shape similar to the 5-ion case, however, it is shifted to larger gate durations: the minimal time for points inside the area is $\sim 60\mu\text{s}$. Analogously with the 5-ion case, we find that $1 - F_0$ is of the order 10^{-5} for Ω_{tr} (see Fig. 3(b)) and of the order of 10^{-2} for Ω_{lin} (see Fig. 3(d)).

For other chain lengths from 2 to 20, we get similar results. In Fig. 5, we show the dependence of the minimal

time t_{min} inside the allowed area on the number of ions. For each n_{ions} , we find the minimal gate duration t_{min}^* for which $1 - F_0$ reaches 10^{-5} . Both of these durations grow monotonically with the increasing number of ions, with t_{min}^* exceeding t_{min} no more than by $\sim 20\mu\text{s}$.

Also, we calculate analytically the spin flip probability for a selected set of points in t_{gate}, μ plane within the allowed area for 5-ion and 20-ion chains for the initial state $|11\rangle_x$. The points are shown as dots in Fig. 3(a) (5 ions) and Fig. 3(b) (20 ions). The values of the spin flip probability are shown in Fig. 3(e) and Fig. 3(f). For all selected points, the spin flip probability for a 5-ion chain does not exceed 10^{-4} , and it is even smaller for a 20-ion chain.

In addition, we perform numerical simulations for a selected set of points shown by dots in Fig. 3(a) for a 5-ion chain. For each pair (t_{gate}, μ) indicated by a dot, we model gate dynamics by solving TDSE with the pulses $\Omega_{\text{lin}}(t)$ and $\Omega_{\text{tr}}(t)$ for the initial states $|11\rangle_z$ and $|11\rangle_x$.

For the initial states $|11\rangle_x$, we calculate the spin flip error as in Section IV. We compared the numerical simulations of the full Hamiltonian, of LD Hamiltonian, and the perturbation theory. The results of these calculations confirm the findings of the Section IV: perturbation theory gives an accurate result for the LD Hamiltonian (2), but the spin flip probability P_{flip}^s is by order of magnitude higher for the full Hamiltonian (1), which is of the order 10^{-5} .

For the initial states $|11\rangle_z$, we perform calculations similar to that of Table I. We compare the analytical zero-order infidelity given by Eq. (23) with the infidelity obtained from TDSE. The results are presented in Fig. 4. For all points, the infidelity for the pulses Ω_{tr} is considerably lower than for Ω_{lin} . By comparing the numerical infidelities for the full Hamiltonian and the LD Hamiltonian, we conclude that the Eq. (23) gives a leading-order contribution to the error for Ω_{lin} . In contrast, the dominant contribution to the error for Ω_{tr} originates from the higher orders of the Lamb-Dicke expansion.

These results show that the conclusions of the Section IV persist for a wide range of these parameters providing that t_{gate} and μ are within the allowed area. Also, the calculations prove that the zero-order error can be reliably used to estimate the fidelity gain given by our scheme.

For gate durations of tens of microseconds, our scheme allows to reduce the gate error from $\sim 10^{-2}$ for non-optimized pulses to $\sim 10^{-5}$. Thus, our scheme facilitates the implementation of fast high-fidelity MS gates in chains with tens of ions, which is crucial for speeding up trapped-ion quantum computation.

V. CONCLUSIONS

We propose an amplitude-pulse-shaping method to shorten the Mølmer-Sørensen entangling gates in linear chains of trapped-ion qubits. Our method allows to con-

siderably reduce the error originating from the carrier transition, which is an intrinsic feature of the ions interaction with bichromatic external field. We show that a certain nonlinear transformation of the laser pulse allows to compensate the modification of the spin-dependent forces by the carrier transition almost entirely, thus enabling a fast high-fidelity gate. For short ion chains, we show analytically and numerically that our method allows to reduce gate infidelity 2-3 orders of magnitude for gate durations of tens of microseconds with the resulting

fidelity below $\sim 10^{-4}$. According to our analytical calculations, these conclusions persist for chains at least up to 20 ions.

ACKNOWLEDGMENTS

This work was supported by Rosatom in the framework of the Roadmap for Quantum computing (Contract No. 868-1.3-15/15-2021).

[1] C. D. Bruzewicz, J. Chiaverini, R. McConnell, and J. M. Sage, Trapped-ion quantum computing: Progress and challenges, *Applied Physics Reviews* **6**, 021314 (2019).

[2] J. I. Cirac and P. Zoller, Quantum computations with cold trapped ions, *Physical Review Letters* **74**, 4091 (1995).

[3] A. Sørensen and K. Mølmer, Entanglement and quantum computation with ions in thermal motion, *Phys. Rev. A* **62**, 022311 (2000).

[4] D. Leibfried, B. DeMarco, V. Meyer, D. Lucas, M. Barrett, J. Britton, W. M. Itano, B. Jelenković, C. Langer, T. Rosenband, and D. J. Wineland, Experimental demonstration of a robust, high-fidelity geometric two ion-qubit phase gate, *Nature* **422**, 412 (2003).

[5] J. Mizrahi, B. Neyenhuis, K. Johnson, W. C. Campbell, C. Senko, D. Hayes, and C. Monroe, Quantum control of qubits and atomic motion using ultrafast laser pulses, *Applied Physics B* **10.1007/s00340-013-5717-6** (2013), arXiv:1307.0557 [physics.atom-ph].

[6] G. Kirchmair, J. Benhelm, F. Zähringer, R. Gerritsma, C. F. Roos, and R. Blatt, Deterministic entanglement of ions in thermal states of motion, *New. J. Phys.* **11**, 023002 (2009) 10.1088/1367-2630/11/2/023002 (2008), arXiv:0810.0670 [quant-ph].

[7] T. Choi, S. Debnath, T. Manning, C. Figgatt, Z.-X. Gong, L.-M. Duan, and C. Monroe, Optimal quantum control of multimode couplings between trapped ion qubits for scalable entanglement, *Physical Review Letters* **112**, 190502 (2014).

[8] A. R. Milne, C. L. Edmunds, C. Hempel, F. Roy, S. Mavadia, and M. J. Biercuk, Phase-modulated entangling gates robust to static and time-varying errors, *Physical Review Applied* **13**, 024022 (2020).

[9] Y. Shapira, R. Shaniv, T. Manovitz, N. Akerman, and R. Ozeri, Robust entanglement gates for trapped-ion qubits, *Physical Review Letters* **121**, 180502 (2018).

[10] N. Grzesiak, R. Blümel, K. Wright, K. M. Beck, N. C. Pisenti, M. Li, V. Chaplin, J. M. Amini, S. Debnath, J.-S. Chen, and Y. Nam, Efficient arbitrary simultaneously entangling gates on a trapped-ion quantum computer, *Nature Communications* **11**, 10.1038/s41467-020-16790-9 (2020).

[11] T. Olsacher, L. Postler, P. Schindler, T. Monz, P. Zoller, and L. M. Sieberer, Scalable and parallel tweezer gates for quantum computing with long ion strings, *PRX Quantum* **1**, 020316 (2020).

[12] R. Blümel, N. Grzesiak, N. Pisenti, K. Wright, and Y. Nam, Power-optimal, stabilized entangling gate between trapped-ion qubits, *npj Quantum Information* **7**, 10.1038/s41534-021-00489-w (2021).

[13] B. P. Ruzic, M. N. Chow, A. D. Burch, D. S. Lobser, M. C. Revelle, J. M. Wilson, C. G. Yale, and S. M. Clark, Leveraging motional-mode balancing and simply parametrized waveforms to perform frequency-robust entangling gates, *Physical Review Applied* **22**, 014007 (2024).

[14] Y. Wu, S.-T. Wang, and L.-M. Duan, Noise analysis for high-fidelity quantum entangling gates in an anharmonic linear paul trap, *Phys. Rev. A* **97**, 062325 (2018).

[15] S. S. Vedaie, E. J. Páez, N. H. Nguyen, N. M. Linke, and B. C. Sanders, Bespoke pulse design for robust rapid two-qubit gates with trapped ions, *Phys. Rev. Res.* **5**, 023098 (2023).

[16] R. Blümel, A. Maksymov, and M. Li, Toward a mølmer sørensen gate with .9999 fidelity, *Journal of Physics B: Atomic, Molecular and Optical Physics* **57**, 205501 (2024).

[17] S. Saner, O. Bazavan, M. Minder, P. Drmota, D. J. Webb, G. Araneda, R. Srinivas, D. M. Lucas, and C. J. Ballance, Breaking the entangling gate speed limit for trapped-ion qubits using a phase-stable standing wave, *Phys. Rev. Lett.* **131**, 220601 (2023).

[18] P. J. Lee, K.-A. Brickman, L. Deslauriers, P. C. Haljan, L.-M. Duan, and C. Monroe, Phase control of trapped ion quantum gates, *Journal of Optics B: Quantum and Semiclassical Optics* **7**, S371 (2005).

[19] O. Băzăvan, S. Saner, M. Minder, A. C. Hughes, R. T. Sutherland, D. M. Lucas, R. Srinivas, and C. J. Ballance, Synthesizing a spin-dependent force for optical, metastable, and ground-state trapped-ion qubits, *Physical Review A* **107**, 022617 (2023).

[20] C. F. Roos, Ion trap quantum gates with amplitude-modulated laser beams, *New Journal of Physics* **10**, 013002 (2008) 10.1088/1367-2630/10/1/013002 (2007), arXiv:0710.1204 [quant-ph].

[21] D. James, Quantum dynamics of cold trapped ions with application to quantum computation, *Applied Physics B: Lasers and Optics* **66**, 181 (1998).

[22] C. Monroe, W. Campbell, L.-M. Duan, Z.-X. Gong, A. Gorshkov, P. Hess, R. Islam, K. Kim, N. Linke, G. Pagano, P. Richerme, C. Senko, and N. Yao, Programmable quantum simulations of spin systems with trapped ions, *Reviews of Modern Physics* **93**, 025001 (2021).

[23] P. C. Haljan, K.-A. Brickman, L. Deslauriers, P. J. Lee, and C. Monroe, Spin-dependent forces on trapped ions

for phase-stable quantum gates and entangled states of spin and motion, *Physical Review Letters* **94**, 153602 (2005).

[24] S.-L. Zhu, C. Monroe, and L.-M. Duan, Arbitrary-speed quantum gates within large ion crystals through minimum control of laser beams, *Europhysics Letters (EPL)* **73**, 485 (2006).

[25] I. Bengtsson and K. Zyczkowski, *Geometry of Quantum States: An Introduction to Quantum Entanglement* (Cambridge University Press, 2006).

[26] J. Johansson, P. Nation, and F. Nori, Qutip 2: A python framework for the dynamics of open quantum systems, *Computer Physics Communications* **184**, 1234 (2013).

[27] M. A. Nielsen and I. L. Chuang, *Quantum Computation and Quantum Information: 10th Anniversary Edition* (Cambridge University Press, 2010).

[28] M. O. Scully and M. S. Zubairy, *Quantum Optics* (Cambridge University Press, 1997).

Appendix A: The MS gate fidelity with account of first-order spin-flip correction

In this Appendix, we derive expressions for the Mølmer-Sørensen gate fidelity with account to three contributions: incompletely closed phonon mode phase trajectories, error in spin coupling phase, and spin-flip contribution. We consider fidelity in the full ion-phonon Hilbert space assuming that all phonon modes are initially cooled to the ground state. So, fidelity F_{tot} is defined by Eq. (21) as squared overlap between the target state and the resulting state. To find F using perturbation theory, it is convenient to denote the combination $R_{XX}^\dagger(\phi)U$ as

$$R_{XX}^\dagger(\phi)\hat{U} = 1 - i\hat{T}. \quad (\text{A1})$$

Using the unitarity of $R_{XX}^\dagger(\phi)\hat{U}$, we can rewrite fidelity in the form more suitable for perturbative calculation:

$$1 - F_{\text{tot}} = \langle \psi_0 | \hat{T}^\dagger \hat{T} | \psi_0 \rangle - \langle \psi_0 | \hat{T} | \psi_0 \rangle^2. \quad (\text{A2})$$

Then, we use the MS gate propagator \hat{U} with the first-order correction from the spin-flip perturbation (18). Let us give a small-error expansion of \hat{T} . We assume that α_{im} and the deviation of χ_{ij} from the target values are small, so the MS propagator can be decomposed as

$$R_{XX}(\phi)^\dagger \hat{U}_0 = \mathbb{1} - i\delta\hat{U}_{\text{MS}}, \quad (\text{A3})$$

where

$$\delta\hat{U}_{\text{MS}} \approx \frac{1}{2} \sum_{i,j} \chi_{ij} \sigma_x^i \sigma_x^j + i \sum_{im} \sigma_x^i (\alpha_{im}^* \hat{a}_m - \alpha_{im} \hat{a}_m^\dagger). \quad (\text{A4})$$

After that, \hat{T} can be approximated as

$$\hat{T} \approx \delta\hat{U}_{\text{MS}} + \hat{T}_1, \quad (\text{A5})$$

where we define \hat{T}_1 by Eq.(19), and neglect the term $\delta U_{\text{MS}} \hat{T}_1$. We find convenient to separate the contributions of $\delta\hat{U}_{\text{MS}}$ and \hat{T}_1 into gate infidelity. For that, we

define two auxiliary fidelities. The first one is the fidelity F_0 of the state obtained by the action of the zero-order evolution operator (14) defined in Section III, Eq. (22). It contains only the contributions of the imperfectly closed phase trajectories and the error in spin coupling phase. The second one is the fidelity between the states $\hat{U}_0|\psi_0\rangle$ and $\hat{U}|\psi_0\rangle$:

$$F_c = |\langle \psi_0 | \hat{U}_0^\dagger \hat{U} | \psi_0 \rangle|^2 \quad (\text{A6})$$

It characterizes the deviation of the full evolution operator \hat{U} from the Mølmer-Sørensen propagator (14) and is determined by \hat{T}_1 . Similarly with (A2), we can express F_0 and F_c as

$$1 - F_0 = \langle \psi_0 | \delta\hat{U}_{\text{MS}}^\dagger \delta\hat{U}_{\text{MS}} | \psi_0 \rangle - |\langle \psi_0 | \delta\hat{U}_{\text{MS}} | \psi_0 \rangle|^2. \quad (\text{A7})$$

and

$$1 - F_c = \langle \psi_0 | \hat{T}_1^\dagger \hat{T}_1 | \psi_0 \rangle - |\langle \psi_0 | \hat{T}_1 | \psi_0 \rangle|^2. \quad (\text{A8})$$

The auxiliary fidelities (22), (A6) are useful for analysing the fidelity F_{tot} (Eq. (21)). First, for any initial state, F_{tot} can be bounded using the triangle inequality for fidelities [27]:

$$F_{\text{tot}} > \cos(\arccos F_0 + \arccos F_c). \quad (\text{A9})$$

Second, let us prove that the infidelity (A2) averaged over initial states is simply a sum of (A7) and (A8). Indeed, the average of (A2) can be calculated as

$$1 - \langle F_{\text{tot}} \rangle = \frac{1}{2^N} \left[\text{Tr}_q \langle 0_{ph} | \hat{T}^\dagger \hat{T} | 0_{ph} \rangle - \text{Tr}_q \langle 0_{ph} | \hat{T}^\dagger | 0_{ph} \rangle \langle 0_{ph} | \hat{T} | 0_{ph} \rangle \right], \quad (\text{A10})$$

where Tr_q denotes the trace over qubit space. Then, we substitute the Eq. (A5) into Eq. (A10). As $\delta\hat{U}_{\text{MS}}$ commutes with all σ_x^i , and \hat{T}_1 contains only terms flipping the pseudospin direction along the x axis, all cross-products of $\delta\hat{U}_{\text{MS}}$ and \hat{T}_1 vanish. Therefore, we get

$$1 - \langle F_{\text{tot}} \rangle = (1 - \langle F_0 \rangle) + (1 - \langle F_c \rangle), \quad (\text{A11})$$

Using Eq. (A10), we get the following expression for $\langle F_0 \rangle$:

$$1 - \langle F_0 \rangle = \sum_{i=1,2} |\alpha_{im}|^2 + \frac{4}{5} \delta\chi_{12}^2. \quad (\text{A12})$$

The contribution F_c averaged over initial states can be bounded from above as an average over all qubit basis states in the x -basis, which simply follows from Eq. (A10):

$$1 - F_c < \frac{1}{4} \text{Tr}_q \hat{T}_1^\dagger \hat{T}_1 = \frac{1}{4} \sum_s \langle s, 0_{ph} | \hat{T}_1^\dagger \hat{T}_1 | s, 0_{ph} \rangle. \quad (\text{A13})$$

A closed-form representation of the term $\langle s, 0_{ph} | \hat{T}_1^\dagger \hat{T}_1 | s, 0_{ph} \rangle$, which is the probability of a

spin flip during the MS gate operation for the initial state $|s, 0_{\text{ph}}\rangle$, is given in Appendix B.

Now let us give expressions for some particular initial states. First of all, let us take the initial state of the form $|s\rangle \otimes |0_{\text{ph}}\rangle$. Similarly with the average fidelity, the action of $\delta\hat{U}_{\text{MS}}$ and \hat{T}_1 in the qubit space implies that the infidelity is a sum of contributions from these operators. We get

$$1 - F_0 = \sum_m \left| \sum_i \alpha_{im} s_i \right|^2, \quad (\text{A14})$$

$$1 - F_c = \langle s, 0_{\text{ph}} | T_1^\dagger T_1 | s, 0_{\text{ph}} \rangle, \quad (\text{A15})$$

$$1 - F_{\text{tot}} = \sum_m \left| \sum_i \alpha_{im} s_i \right|^2 + \langle s, 0_{\text{ph}} | T_1^\dagger T_1 | s, 0_{\text{ph}} \rangle. \quad (\text{A16})$$

Here $\delta\chi_{ij}$ does not contribute into error as it is responsible only for the phase between different qubit basis vectors in x -basis.

Finally, let us give expressions for F_0 for the initial state $|\psi_0\rangle = |s\rangle_z \otimes |0_{\text{ph}}\rangle$ (a spin string in z -basis) and for an arbitrary superposition of qubit states in x basis:

$$|\psi_0\rangle = \sum c_s |s\rangle \otimes |0_{\text{ph}}\rangle. \quad (\text{A17})$$

For $|\psi_0\rangle = |s\rangle_z \otimes |0_{\text{ph}}\rangle$,

$$1 - F_0 = \sum_{i=1,2} |\alpha_{im}|^2 + \delta\chi_{12}^2. \quad (\text{A18})$$

For a superposition with arbitrary coefficients c_s ,

$$1 - F_0 = \sum_s |c_s|^2 |\alpha^T s|^2 + \frac{1}{4} \sum_s |c_s|^2 (s^T \delta\chi s)^2 - \frac{1}{4} \left| \sum_s |c_s|^2 (s^T \delta\chi s) \right|^2. \quad (\text{A19})$$

The expressions for F_0 for the latter states can be obtained in the same way. In general, they contain the interference terms coming from products of $\delta\hat{U}_{\text{MS}}$ and \hat{T}_1 .

Appendix B: Spin flip probability

In this Appendix, we derive a closed-form representation of the probability of a spin flip during the MS gate operation for the initial state $|s, 0_{\text{ph}}\rangle$, which is given by the matrix element $\langle s, 0_{\text{ph}} | \hat{T}_1^\dagger \hat{T}_1 | s, 0_{\text{ph}} \rangle$. We represent it as a two-dimensional integral. From Eq. (19), we get

$$\hat{T}_1^\dagger \hat{T}_1 = \int dt' dt'' \hat{U}_0^\dagger(t', t_0) \hat{V}(t') \hat{U}_0(t', t'') \hat{V}(t'') \hat{U}_0(t'', t_0). \quad (\text{B1})$$

The propagator \hat{U}_0 given by Eq. (14) is diagonal in qubit space and contains displacement operators in phonon space and can be represented as

$$\hat{U}_0(t_2, t_1) = \sum e^{-i\chi_s(t_2, t_1)} D(\alpha^T(t_2, t_1)s) |s\rangle \langle s|, \quad (\text{B2})$$

where $\alpha(t_2, t_1)$ is the matrix $\alpha_{im}(t_2, t_1)$, and

$$\chi_s(t_2, t_1) = \frac{1}{2} \sum_{ij} \chi_{ij}(t_2, t_1) s_i s_j. \quad (\text{B3})$$

The perturbation \hat{V} can be written as

$$\hat{V}(t) = \sum \hat{V}_m^\beta(t) A_m^\beta, \quad \beta = 1, 2, \quad (\text{B4})$$

with

$$\begin{aligned} \hat{A}_m^1 &= \hat{a}_m, \\ \hat{A}_m^2 &= \hat{a}_m^\dagger, \end{aligned} \quad (\text{B5})$$

$$V_m^\beta(t) = \sum_i V_{im}^\beta(t) \sigma_z^i, \quad (\text{B6})$$

$$V_{im}^{1,2}(t) = \eta_{im} \Omega(t) \cos(\mu t + \psi) \sin 2\Phi(t) e^{\mp i\omega_m t}. \quad (\text{B7})$$

By substituting these expressions into Eq. (B1) and taking the required matrix element, one gets

$$\begin{aligned} \langle s, 0_{\text{ph}} | \hat{T}_1^\dagger \hat{T}_1 | s, 0_{\text{ph}} \rangle = & \sum_{i, m_1, m_2, \beta_1, \beta_2, s'} \int dt_1 dt_2 (V_{m_1}^{\beta_1})_{ss'}(t_1) (V_{m_2}^{\beta_2})_{ss'}(t_2) e^{i(\chi_s(t_1, t_0) - \chi_{s'}(t_1, t_2) + \chi_s(t_2, t_0))} \\ & \langle 0_{\text{ph}} | D^\dagger(\alpha^T(t_1, t_0)s) \hat{A}_{m_1}^{\beta_1} D(\alpha^T(t_1, t_2)s') \hat{A}_{m_2}^{\beta_2} D(\alpha^T(t_2, t_0)s) | 0_{\text{ph}} \rangle. \end{aligned} \quad (\text{B8})$$

The matrix elements of the products of displacement op-

erators and creation and annihilation operators can be

calculated using the identities for displacement operators (see, for example, [28]). Below we give the expressions for

$$\begin{aligned}
\langle 0_{\text{ph}} | D^\dagger(\vec{\alpha}) \hat{a}_{m_1} D(\vec{\alpha}_2) \hat{a}_{m_2} D(\vec{\alpha}_3) | 0_{\text{ph}} \rangle &= \langle 0_{\text{ph}} | D^\dagger(\vec{\alpha}_1) D(\vec{\alpha}_2) D(\vec{\alpha}_3) | 0_{\text{ph}} \rangle ((\alpha_2)_{m_1} + (\alpha_3)_{m_1})(\alpha_3)_{m_2}, \\
\langle 0_{\text{ph}} | D^\dagger(\vec{\alpha}_1) \hat{a}_{m_1} D(\vec{\alpha}_2) \hat{a}_{m_2}^\dagger D(\vec{\alpha}_3) | 0_{\text{ph}} \rangle &= \langle 0_{\text{ph}} | D^\dagger(\vec{\alpha}_1) D(\vec{\alpha}_2) D(\vec{\alpha}_3) | 0_{\text{ph}} \rangle (\alpha_1^*)_{m_1} (\alpha_3)_{m_3}, \\
\langle 0_{\text{ph}} | D^\dagger(\vec{\alpha}_1) \hat{a}_{m_1}^\dagger D(\vec{\alpha}_2) \hat{a}_{m_2} D(\vec{\alpha}_3) | 0_{\text{ph}} \rangle &= \langle 0_{\text{ph}} | D^\dagger(\vec{\alpha}_1) D(\vec{\alpha}_2) D(\vec{\alpha}_3) | 0_{\text{ph}} \rangle (\delta_{m_1 m_2} + ((\alpha_1)_{m_2}^* - (\alpha_2)_{m_2}^*) ((\alpha_2)_{m_1} + (\alpha_3)_{m_1})), \\
\langle 0_{\text{ph}} | D^\dagger(\vec{\alpha}_1) \hat{a}_{m_1}^\dagger D(\vec{\alpha}_2) \hat{a}_{m_2}^\dagger D(\vec{\alpha}_3) | 0_{\text{ph}} \rangle &= \langle 0_{\text{ph}} | D^\dagger(\vec{\alpha}_1) D(\vec{\alpha}_2) D(\vec{\alpha}_3) | 0_{\text{ph}} \rangle (\alpha_1)_{m_1}^* ((\alpha_1)_{m_2}^* - (\alpha_2)_{m_2}^*), \\
\langle 0_{\text{ph}} | D^\dagger(\vec{\alpha}_1) D(\vec{\alpha}_2) D(\vec{\alpha}_3) | 0_{\text{ph}} \rangle &= \exp \left\{ -i \text{Im}[(\vec{\alpha}_1 \vec{\alpha}_2^*) + (\vec{\alpha}_1 \vec{\alpha}_3^*) - (\vec{\alpha}_2 \vec{\alpha}_3^*)] - \frac{1}{2} |\alpha_1 - \alpha_2 - \alpha_3|^2 \right\}.
\end{aligned} \tag{B9}$$

Appendix C: Averaging the spin-dependent force over fast carrier oscillations

The integrals for α_{im} and χ_{ij} entering the MS propagator (Eqs. (15) and (16)) contain the term f_{im} (Eq.(17)) with a fastly-oscillating multiplier $\cos 2\Phi(t)$. Here we show how the fast oscillations can be approximately averaged on the timescale $\sim \mu^{-1}$. For that, let us explicitly decompose f_{im} as a product of slowly and fastly varying components:

$$f_{im}(t) = \underbrace{\frac{1}{2} \eta_{im} e^{i(\omega_m - \mu)t - i\psi} \Omega(t)}_{\text{slow part}} \underbrace{(1 + e^{2i(\mu t + \psi)}) \cos 2\Phi(t)}_{\text{fast part}} \tag{C1}$$

We assume that the slow part does not change significantly over several periods of carrier oscillations μ^{-1} . Then, we can average the fast part assuming that $\Omega(t)$ is approximately constant. Also, due to the assumptions on $\Omega(t)$ made in Section IV, we can replace $\Phi(t)$ by the leading-order asymptotic contribution:

$$\Phi(t) = \int_{t_0}^t dt' \Omega(t') \cos(\mu t' + \psi) \approx \frac{\Omega(t)}{\mu} \sin(\mu t + \psi). \tag{C2}$$

After that, the fast part can be averaged as follows:

$$\begin{aligned}
\left\langle (1 + e^{2i(\mu t + \psi)}) \cos \left(\frac{2\Omega}{\mu} \sin(\mu t + \psi) \right) \right\rangle &= \\
&= J_0 \left(\frac{2\Omega}{\mu} \right) + J_2 \left(\frac{2\Omega}{\mu} \right), \tag{C3}
\end{aligned}$$

where J_n are Bessel functions.

By substituting (C3) into (C1), we get

$$\begin{aligned}
f_{im}(t) &\approx \frac{1}{2} \eta_{im} e^{i(\omega_m - \mu)t - i\psi} \Omega(t) \times \\
&\quad \underbrace{\left(J_0 \left(\frac{2\Omega(t)}{\mu} \right) + J_2 \left(\frac{2\Omega(t)}{\mu} \right) \right)}_{\text{averaged fast part}} \tag{C4}
\end{aligned}$$

the matrix elements for all combinations of β , which corresponds to all combinations of creation and annihilation operators:

Due to smooth time dependence of $\Omega(t)$, we can replace the oscillating exponent with the cosine and obtain the Eq. (28).

Appendix D: Normal modes of a linear trapped-ion crystal

For a linear ion chain in a harmonic Paul trap potential, the equilibrium positions can be found from numerical minimization of the potential energy

$$U = \sum_k \frac{m\omega_{\text{ax}}^2 x_k^2}{2} + \sum_{k < l} \frac{e^2}{4\pi\epsilon_0 |x_k - x_l|}. \tag{D1}$$

Then, normal modes and frequencies can be found from the second-order expansion of the potential near the equilibrium positions. For the axial (radial) modes, the eigenfrequencies ω_{ax}^m (ω_{rad}^m) and the normal vectors b_{im}^{ax} (b_{im}^{rad}) can be found from the following eigenvalue problems:

$$\sum_l \left[M\omega_{\text{ax}}^2 \delta_{kl} + \frac{e^2}{2\pi\epsilon_0} \tilde{G}_{kl} \right] b_{lm}^{\text{ax}} = m(\omega_m^{\text{ax}})^2 b_{km}^{\text{ax}}, \tag{D2}$$

$$\sum_l \left[M\omega_{\text{rad}}^2 \delta_{kl} - \frac{e^2}{4\pi\epsilon_0} \tilde{G}_{kl} \right] b_{lm}^{\text{rad}} = M(\omega_m^{\text{rad}})^2 b_{km}^{\text{rad}}, \tag{D3}$$

where \tilde{G}_{ij} is the Hessian matrix of the Coulomb potential:

$$\tilde{G}_{kl} = \sum_{k'} \frac{1}{|x_k - x_{k'}|^3} \delta_{kl} - \frac{1}{|x_k - x_l|^3}. \tag{D4}$$

The Lamb-Dicke parameters for the axial and radial normal modes are defined as

$$\tilde{\eta}_{km}^{\text{ax}} = k_{\text{ax}} \sqrt{\frac{\hbar}{2M\omega_m^{\text{ax}}}} b_{km}^{\text{ax}}, \tag{D5}$$

$$\tilde{\eta}_{km}^{\text{rad}} = k_{\text{rad}} \sqrt{\frac{\hbar}{2M\omega_m^{\text{rad}}}} b_{km}^{\text{rad}}, \tag{D6}$$

where k_{ax} (k_{rad}) is the laser wavevector component in axial (radial) direction. Only a part of the full Lamb-Dicke parameter matrix which corresponds to the illuminated ions enters the laser-ion Hamiltonian (1). Let (k_1, k_2) be two ions for which the MS gate is implemented. Then, we define the matrix η_{im} used in the main text as

$$\eta_{im} = \eta_{k_i m}^{\text{rad}}, \quad i = 1, 2. \quad (\text{D7})$$

Appendix E: Pulse shaping with piecewise-polynomial pulses

As a first step of the pulse shaping procedure of the Section IV A, one needs to find $\Omega(t)$ which satisfies the Eqs. (9) and (10). These equations comprise a system of $2n_{\text{ions}}$ linear equations and a single quadratic equation on $\Omega(t)$. The finite set of equations on a continuous function $\Omega(t)$ cannot define it uniquely, so additional constraints should be imposed on $\Omega(t)$.

Assume that $\Omega(t)$ is decomposed into a basis set $\{b_s(t)\}$, $\Omega(t) = \sum_s \Omega_s b_s(t)$, where the functions $b_s(t)$ are defined on the interval (t_0, t_f) of the gate duration. Then, the equations $\alpha_{im} = 0$ reduce to a linear system [14]

$$\sum_s A_{ms} \Omega_s = 0, \quad (\text{E1})$$

where

$$A_{ms} = \int_{t_i}^{t_f} dt b_s(t) \cos(\mu t + \psi) e^{i\omega_m t}, \quad (\text{E2})$$

and the equation $\chi_{12}(t_f) = \phi$ reduces to a quadratic equation

$$\sum_{ss'} B_{ss'} \Omega_s \Omega_{s'} = \frac{\pi}{4}, \quad (\text{E3})$$

where

$$B_{ss'} = - \sum_m 2\eta_{1m} \eta_{2m} \int_{t_i}^{t_f} dt \int_{t_i}^t dt' b_s(t) b_s(t') \times \cos(\mu t + \psi) \cos(\mu t' + \psi) \sin[\omega_m(t - t')] \quad (\text{E4})$$

In order to ensure the smoothness conditions necessary for the consideration of Section IV, we search for $\Omega(t)$ in form of a cubic spline defined by its values in the points t_s evenly spaced in the interval (t_0, t_f) , $t_s = t_0 + \frac{(t_f - t_0)s}{n_{\text{seg}} + 1}$, where $s = 0, \dots, n_{\text{seg}} + 1$. The basis functions $b_s(t)$ are defined as cubic splines on the interval (t_0, t_f) satisfying the boundary conditions $b_s(t_0) = b_s(t_f) = 0$, $b'_s(t_0) = b'_s(t_f) = 0$ and the conditions $b_s(t_{s'}) = \delta_{s,s'}$, $s = 1 \dots n_{\text{seg}}$.